J Pathol Inform

Editor-in-Chief:
Anil V. Parwani , Pittsburgh, PA, USA
Liron Pantanowitz, Pittsburgh, PA, USA

OPEN ACCESS
HTML format

For entire Editorial Board visit : www.jpathinformatics.org/editorialboard.asp

Original Article

Full-field optical coherence tomography for the analysis of fresh unstained human lobectomy specimens

Manu Jain[1,2], Navneet Narula[3], Bekheit Salamoon[2], Maria M. Shevchuk[3], Amit Aggarwal[2#], Nasser Altorki[4], Brendon Stiles[4], Claude Boccara[5,6], Sushmita Mukherjee[2]

Departments of [1]Urology, [2]Biochemistry, [3]Pathology and Laboratory Medicine and [4]Cardiothoracic Surgery, Weill Medical College of Cornell University, New York, USA, [5]Langevin Institute, at ESPCI (1 rue Jussieu, 75005 Paris, France), [6]LLTech, at Cochin Hospital's Business Incubator (29 rue du Faubourg Saint-Jacques, 75014 Paris, France), [#]Department of Science, Borough of Manhattan Community College, New York, NY, USA

E-mail: *Sushmita Mukherjee - smukherj@med.cornell.edu
*Corresponding author

Received: 23 May 13 Accepted: 27 July 13 Published: 27 September 2013

This article may be cited as:
Jain M, Narula N, Salamoon B, Shevchuk MM, Aggarwal A, Altorki N, *et al*. Full-field optical coherence tomography for the analysis of fresh unstained human lobectomy specimens. J Pathol Inform 2013;4:26.

Available FREE in open access from: http://www.jpathinformatics.org/text.asp?2013/4/1/26/119004

Copyright: © 2013 Jain M. This is an open-access article distributed under the terms of the Creative Commons Attribution License, which permits unrestricted use, distribution, and reproduction in any medium, provided the original author and source are credited.

Abstract

Background: Full-field optical coherence tomography (FFOCT) is a real-time imaging technique that generates high-resolution three-dimensional tomographic images from unprocessed and unstained tissues. Lack of tissue processing and associated artifacts, along with the ability to generate large-field images quickly, warrants its exploration as an alternative diagnostic tool. **Materials and Methods:** One section each from the tumor and from adjacent non-neoplastic tissue was collected from 13 human lobectomy specimens. They were imaged fresh with FFOCT and then submitted for routine histopathology. Two blinded pathologists independently rendered diagnoses based on FFOCT images. **Results:** Normal lung architecture (alveoli, bronchi, pleura and blood vessels) was readily identified with FFOCT. Using FFOCT images alone, the study pathologists were able to correctly identify all tumor specimens and in many cases, the histological subtype of tumor (e.g., adenocarcinomas with various patterns). However, benign diagnosis was provided with high confidence in roughly half the tumor-free specimens (others were diagnosed as equivocal or false positive). Further analysis of these images revealed two major confounding features: (a) Extensive lung collapse and (b) presence of smoker's macrophages. On a closer inspection, however, the smoker's macrophages could often be identified as distinct from tumor cells based on their relative location in the alveoli, size and presence of anthracosis. We posit that greater pathologist experience, complemented with morphometric analysis and color-coding of image components, may help minimize the contribution of these confounders in the future. **Conclusion:** Our study provides evidence for the potential utility of FFOCT in identifying and differentiating lung tumors from non-neoplastic lung tissue. We foresee its potential as an adjunct to intra-surgical frozen section analysis for margin assessment, especially in limited lung resections.

Key words: Full-field optical coherence tomography, histopathology, lobectomy, neoplastic tissue

Access this article online

Website: www.jpathinformatics.org

DOI: 10.4103/2153-3539.119004

Quick Response Code:

INTRODUCTION

Lung cancer is the second most common cancer in both men and women. In 2012, it accounted for ~14% of all new cases and 28% of cancer deaths in the United States.[1] Routinely, lung tumors are detected on chest X-rays and computed tomography scans. Biopsies are then obtained from the suspicious lesions and submitted for histopathological confirmation. For the surgical management of patients with small tumors and those with already compromised lung function, smaller wedge resections are preferred over the more radical lobectomies. These resection specimens are typically sent for intrasurgical frozen section analysis (FSA) to confirm negative surgical margins.[2]

Although histopathological analysis and FSA are considered to be the gold standard in diagnosis and management of tumors, they are nevertheless fraught with significant limitations. These limitations mainly arise from tissue processing (freezing, sectioning and staining) that causes artifacts and may lead to false/non-interpretable diagnosis.[3] Tissue processing is also time consuming, delaying pathology feedback on FSAs. This in turn increases surgical time, with associated increases in morbidity and cost for the patient.[4]

To overcome obstacles associated with tissue processing involved in traditional frozen section histopathology, efforts have been focused on high-resolution optical biopsy techniques that can generate histology quality images from fresh (unprocessed and unstained) tissue at relatively fast speeds (so-called "optical biopsy" techniques). One such technique is full-field optical coherence tomography (FFOCT).[5,6] FFOCT is based on the principle of white light interference microscopy. It uses a simple tungsten halogen lamp, which is potentially safer than laser-based light sources used in other optical biopsy techniques including traditional optical coherence tomography (OCT), as well as confocal and multiphoton microscopy. In addition, it can capture the entire field-of-view at once with the charge-coupled device (CCD) or a complementary metal oxide semiconductor (CMOS) camera and thus, does not require raster scanning of a focused laser beam as used in confocal or multiphoton microscopy. The optical arrangement is generally based on a bulk Michelson interferometer, with identical microscope objectives in both arms. This configuration is referred to as the Linnik interferometer[7] [Figure 1]. When a biological object is placed under the objective in the object arm, the light reflected by the reference mirror interferes with the light reflected or backscattered by the sample structures contained in a limited volume, which is recorded by a detector array (CCD or a CMOS camera) and utilized to generate an en-face tomographic image. FFOCT has been previously utilized to assess histological features of *ex vivo* tissues,[8-10] including those of rat lung.[8,11] Recently, a miniaturized probe-based FFOCT prototype has been used for both *ex vivo* (breast) and preliminary *in vivo* skin imaging in human specimens.[12]

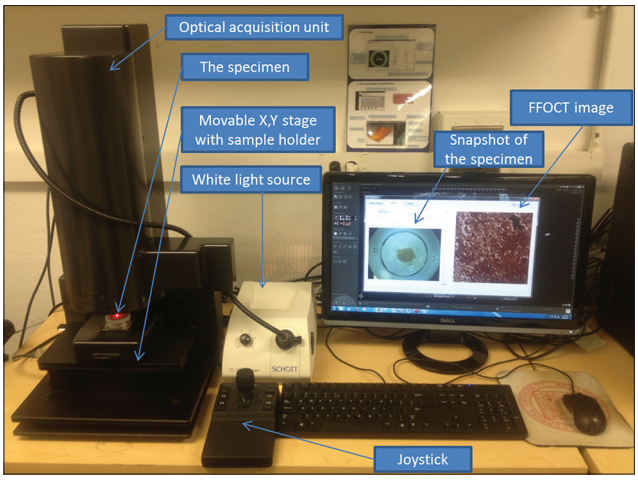

Figure 1: Full-field optical coherence tomography instrumentation. A photograph showing the layout of different components of the LLTech light-collisional thick target model system

In this study, we have explored the potential of FFOCT to identify and differentiate neoplastic from adjacent non-neoplastic lung tissue in fresh *ex vivo* human lobectomy specimens. The goal was to determine its applicability in a clinical context, utilizing the commercial FFOCT device from LLTech, Inc., Light-CT™.

MATERIALS AND METHODS

Study Cohort

A total of 13 adult subjects diagnosed with lung cancer and undergoing lobectomies at our institution participated in the Institutional Review Board approved the study.

Specimen Acquisition and Handling

The 13 lobectomy specimens received in surgical pathology were grossed and inked for tumor margin. Then, one section each (approximately 3 mm × 3 mm × 0.5 mm) from the tumor and tumor-free area (total of 26 samples) were collected fresh in cold buffered saline and brought to the FFOCT facility for imaging. Following FFOCT imaging, the specimens were placed in 10% buffered formalin and submitted for routine histopathological examination.

Sample Preparation

The samples to be imaged were immersed in an isotonic solution of phosphate-buffered saline (PBS; 2.7 mm potassium chloride and 137 mm sodium chloride; pH 7.5) and placed in a sample holder (provided with the Light-CT™ system), with the surface to be imaged oriented upward. A silica cover-slip was placed on top

of the sample and the base of the holder was gently moved upward, so the sample was slightly flattened. This provided an even imaging surface and also expelled any air bubbles.

FFOCT Instrumentation

A commercial FFOCT system was used (light-CT™ scanner, LLTech, France). It is a modified FFOCT system, which has high resolution (1.5 μm transverse and 0.8 μm axial) as compared to the traditional OCT systems, using a spatially and temporally incoherent light source of low power (Quartz-Halogen Schott KL 1500 Compact, Mainz, Germany). Transverse en-face tomographic images of the samples are obtained by the combination of interferential images acquired by a CMOS camera. The native field of view is 0.8 mm by 0.8 mm; however larger fields of view can be acquired by image tiling. The system is also able to collect 3-dimensional image stacks through the top ~60 μm of the specimen (the precise penetration depth varies with specimen type). The microscope utilizes two matched 10×/0.3 NA water immersion objectives (Olympus America, Center Valley, PA), one to collect reflections and backscattering signals from the specimen and the other to collect reflection signal from a reference mirror. The instrument design and the light path are shown in Figure 1.

Image Acquisition and Processing

A thick layer of silicone oil was applied on the silica cover-slip as the objective immersion medium (with the specimen gently flattened underneath as described above). The objective lens was focused on the areas of interest in the sample through a motorized adjustment of the whole interferometer. All specimens were imaged starting at the surface of the tissue in 5-10 μm increments, until the deepest part of the tissue where meaningful signals could still be obtained. This, for human lung tissue, was found to be 50-60 μm. In most cases, the image quality for diagnostic purposes was found to be optimal 5-15 μm below the specimen surface. Imaging of a 2.72 mm × 2.72 mm field-of-view with 10 optical sections, reaching a depth of 50-60 μm within the tissue (representing a typical sample imaging session), took ~7 min. Two to eight images were acquired from different areas in a given sample, depending on the size of the specimen and the complexities observed in the tissue architecture. The images were processed in real time with a digital imaging and communication in medicine viewer and saved. They were read and further processed with Image J software (National institutes of Health, Bethesda, MD), if necessary. Speckle noise was minimized using Gaussian filtering in Adobe Photoshop CS5 (San Jose, CA).

Histopathologic Diagnosis Using FFOCT Images

To assess the diagnostic capabilities of FFOCT for lung cancer, all FFOCT images and Hematoxylin and Eosin (H&E)-stained slides prepared from the same specimen, were reviewed by two pathologists (a pulmonary pathologist and a general pathologist).

Training Set

The pathologists were first familiarized with the appearance of specific histological features on FFOCT using a "training set" of images. For this training set, representative image, six each from non-neoplastic and neoplastic lung tissues were selected. Although these training images came from the same 13 subjects, the specific images used in the training set were excluded from the blinded study to prevent any bias. Further, corresponding H&E slides were made available to assist with feature recognition on FFOCT. It took roughly a half hour to train each pathologist on interpreting the FFOCT images. It is important to note here that both pathologists in this study have substantial experience in interpreting images obtained from other novel imaging modalities (e.g., multiphoton microscopy). It is likely that the training will take longer for pathologists who have no experience working with images from these novel imaging techniques.

Test Set

After this initial training, the pathologists were presented the rest of the FFOCT images alone in a blinded fashion. In all cases, the pathologists were asked to score the images as neoplastic or non-neoplastic. For many tumor specimens, they additionally commented on the histological tumor type (e.g., lepidic vs. solid adenocarcinomas). H&E-stained sections from the same specimens were subsequently reviewed by the same pathologist, to confirm their diagnosis and to assess the reasons for misdiagnosis when it happened.

Each pathologist reviewed a total of 41 test image sets. In some cases, they were able to diagnose based on just one chosen image (typically one taken 5-5 μm below the specimen surface), whereas in other cases, they chose to also review the entire image stack (from the tissue surface to ~60 μm deep). It took approximately 1.5 h for each pathologist to render diagnoses on all 41 test images.

Because of the small sample size in this study, we have not presented a formal diagnostic accuracy analysis. Table 1 shows detailed diagnostic performance of FFOCT in lung lesions.

RESULTS

FFOCT Can Recapitulate Normal Histology of Human Lung Tissue

To assess the ability of FFOCT to identify lung tumor, we first assessed the images from the non-neoplastic lung tissue adjacent to the tumor. In non-neoplastic lung tissue, we could easily recognize the typical lace-like pattern of lung parenchyma formed by

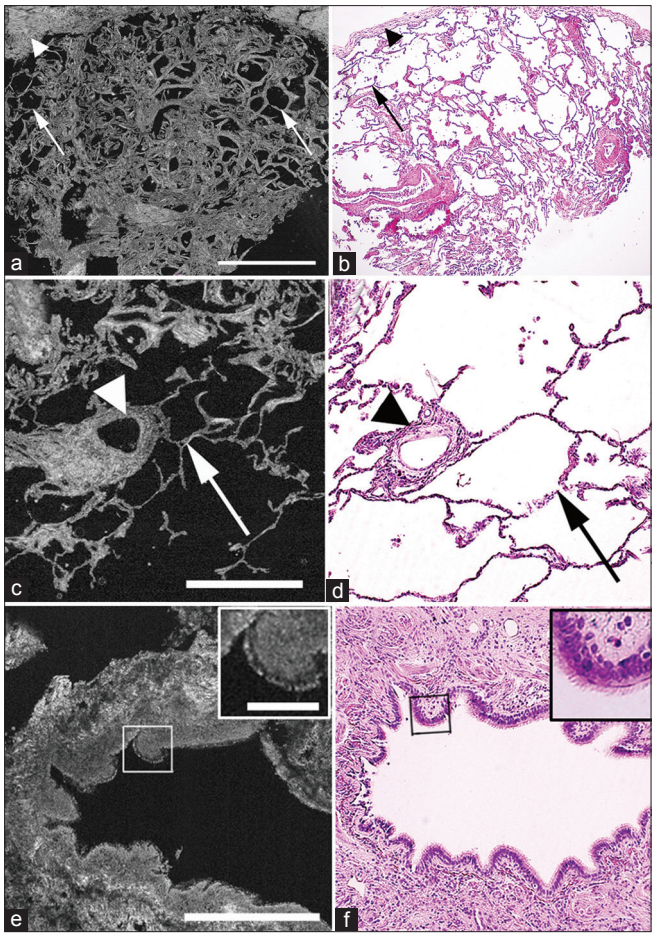

Figure 2: Comparative full-field optical coherence tomography (FFOCT) and H&E images of non-neoplastic lung. (a, b) Large-field images show lung parenchyma composed of alveoli (signal void areas; arrows) surrounded by pleura (connective tissue-bright signals; arrowheads). Some thickening of the alveolar septa is shown (right arrow). (c, d) Images of blood vessel (arrowheads) and surrounding alveoli (arrows). (e, f) Images of a bronchus, with columnar epithelial lining (box and inset) and underlying connective tissue (connective tissue-bright signal). (Scale bars for FFOCT: (a) 1 mm; (c, e) 0.5 mm. Inset in (e) 0.1 mm. H&E total magnifications: (b) ×40 and (d, f) ×200. Inset in (f) = ×2.5 zoom)

alveoli (signal-void dark areas), along with their septal walls (bright signal) [Figure 2a and b]. Since the non-neoplastic tissues were taken from an area adjacent to lung tumor, some emphysematous changes (loss and thickening of the alveolar septa) were observed in these sections [Figure 2a and b]. We could also readily identify the following other major normal lung components: (A) Pleura, which is rich in connective tissue and produces a bright signal [Figure 2a and b]; (B) blood vessels [Figure 2c and d] and (C) bronchi, with their columnar epithelial lining (the cells generating a dull gray signal) [Figure 2e and f].

FFOCT Can Identify Neoplastic Lung Tissue with High Reliability

After identifying the normal components of lung, we assessed images from sections containing lung tumors. When presented to two independent pathologists in a blinded manner, they were able to identify all images, which contained tumor correctly. In addition to identifying tumor, we could also recognize various histological patterns of tumors in the FFOCT images, especially for adenocarcinomas. For example, more differentiated adenocarcinomas with predominant lepidic pattern (cells growing along the alveolar septa) [Figure 3a and b] were distinguishable from invasive tumor with predominant solid pattern (clusters of cells) [Figure 3c and d]. The tumor cells appeared to have a dull gray signal, similar to other normal cells [e.g. those lining the bronchi, Figure 2e and f], but were distinguished from normal cells by their size and arrangement.

Pathological Diagnosis Based on FFOCT was Confounded by Collapsed Lung and the Presence of Smokers' Macrophages

When the same pathologists who could identify the presence of lung tumors in all cases were presented images from tumor-free areas of the lung, they could provide a benign diagnosis with high confidence in roughly half of the cases. For the remaining tumor-free lung specimens, the diagnosis was either equivocal or false positive. Further analysis of these images revealed two major confounding features.

a. Extensive lung collapse [Figure 4a and b]. Using the FFOCT images alone, the pathologists could not confidently distinguish between collapsed benign lung tissue and areas filled with tumor cells, since both looked dense, with similar contrasts, on FFOCT.
b. The presence of abundant inflammatory cells (smoker's macrophages) [Figure 4c and d]. When the macrophages filled the alveolar spaces, they bore some resemblance to solid tumor growth. On a closer inspection, however, the smoker's macrophages could often be identified as distinct from tumor cells since they localized in the alveolar spaces (and not along the wall) and appeared bigger in size with abundant cytoplasm [Figure 4c and d]. In some of the images, smoker's macrophages contained bright spots in their cytoplasm, which could be due to the presence of anthracosis [inset in Figure 4c]. Thus, with more experience, these unique signals on FFOCT may help the pathologists distinguish inflammatory cells from tumor cells.

DISCUSSION

In this first-of-its-kind study, we investigate the potential use of FFOCT in real-time evaluation of lung tumors in fresh (unprocessed and unstained) human lobectomy specimens. We have demonstrated the ability of FFOCT not only to recapitulate the normal histology of lung, but also to identify and differentiate lung tumors from non-neoplastic lung tissue.

Table 1: Diagnostic performance of FFOCT for lung lesions

No. of Images	Pathological diagnosis on H&E sections	FFOCT diagnosis		Causes for false diagnosis
		Pathologist 1	Pathologist 2	
1	Non neoplastic	Adenocarcinoma with LPP	Non neoplastic	Collapsed lung parenchyma
2	Non neoplastic	Non neoplastic	Non neoplastic	
3	Adenocarcinoma with APP	Adenocarcinoma with APP	Adenocarcinoma with APP	
4	Adenocarcinoma with APP moderately-poorly differentiated	Adenocarcinoma with APP	Adenocarcinoma with APP	
5	Non neoplastic	Adenocarcinoma, pattern not identified	Adenocarcinoma with LPP	Collapsed lung parenchyma, histiocytes
6	Adenocarcinoma with APP moderately-poorly differentiated	Adenocarcinoma with APP	Adenocarcinoma with APP	
7	Non neoplastic	Adenocarcinoma with LPP	Adenocarcinoma with LPP	Reactive proliferative pneumocytes and macrophage proliferation
8	Adenocarcinoma poorly differentiated	Adenocarcinoma with SPP	Adenocarcinoma with SPP	
9	Adenocarcinoma with LPP	Adenocarcinoma with LPP	Adenocarcinoma with LPP	
10	Non neoplastic	Non neoplastic	Non neoplastic	
11	Adenocarcinoma with LPP	Adenocarcinoma with LPP	Adenocarcinoma with LPP	
12	Adenocarcinoma with APP, moderately differentiated.	Adenocarcinoma with APP	Adenocarcinoma with APP	
13	Non neoplastic	Non neoplastic	Adenocarcinoma with LPP	Tangential placement of the tissue can mimic lepidic pattern with thick septa
14	Adenocarcinoma with APP	Adenocarcinoma with APP	Adenocarcinoma with APP	
15	Non neoplastic	Non neoplastic	Non neoplastic	
16	Adenocarcinoma with APP, moderately differentiated.	Adenocarcinoma with APP	Adenocarcinoma with APP	
17	Adenocarcinoma with APP	Adenocarcinoma. Pattern not sure	Adenocarcinoma, possible Acinar	
18	Keratinizing, well differentiated Squamous cell carcinoma	Solid tumor	Solid tumor	
19	Adenocarcinoma with LPP	Adenocarcinoma with LPP	Adenocarcinoma with LPP	
20	Non neoplastic	Non neoplastic	Non neoplastic	
21	Moderately-differentiated, Invasive squamous cell carcinoma	Solid tumor	Solid tumor	
22	Non neoplastic	Non neoplastic	Non neoplastic	
23	Non neoplastic	Non neoplastic	Non neoplastic	
24	Squamous cell carcinoma	Solid tumor	Solid tumor	
25	Squamous cell carcinoma	Solid tumor	Solid tumor	
26	Squamous cell carcinoma	Solid tumor	Solid tumor	
27	Non neoplastic	Adenocarcinoma with LPP	Adenocarcinoma with LPP	Reactive proliferative pneumocytes and macrophage proliferation
28	Non neoplastic	Adenocarcinoma with LPP	Non neoplastic	
29	Non neoplastic	Adenocarcinoma with LPP	Adenocarcinoma with LPP	Thickened lobular septa with macrophages
30	Non neoplastic	Adenocarcinoma with LPP	Adenocarcinoma with LPP	Thickened lobular septa with macrophages
31	Adenocarcinoma with APP	Adenocarcinoma, solid and acinar pattern	Adenocarcinoma with APP	
32	Non neoplastic	Non neoplastic	Non neoplastic	
33	Non neoplastic	Non neoplastic	Non neoplastic	
34	Non neoplastic	Adenocarcinoma	Non neoplastic	Collapsed lung
35	Squamous cell carcinoma	Solid tumor, possible adenocarcinoma	Solid tumor	
36	Squamous cell carcinoma	Solid tumor, possible adenocarcinoma	Solid Tumor	

contd...

Table 1: Contd...

No. of Images	Pathological diagnosis on H&E sections	FFOCT diagnosis		Causes for false diagnosis
		Pathologist 1	Pathologist 2	
37	Non neoplastic	Tumor	Non neoplastic	Collapsed lung
38	Non neoplastic	Non neoplastic	Non neoplastic	
39	Adenocarcinoma with SPP poorly differentiated	Tumor	Tumor	
40	Adenocarcinoma with SPP poorly differentiated	Tumor	Tumor	
41	Non neoplastic	Adenocarcinoma with LPP	Adenocarcinoma with LPP	Thickened lobular septa with macrophages

FFOCT: Full-field optical coherence tomography, LPP: Lepidic predominant pattern, APP: Acinar predominant pattern, SPP: Solid predominant

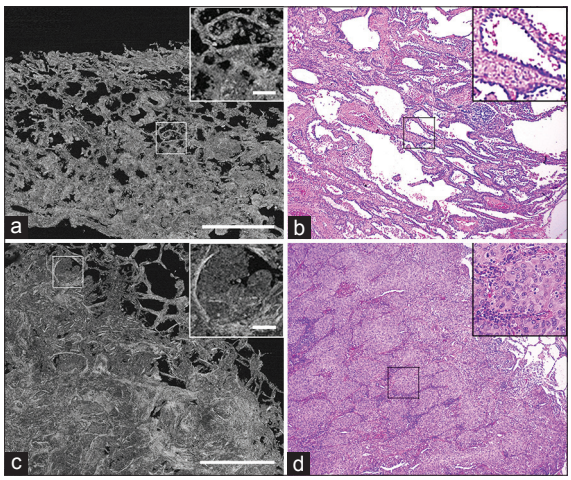

Figure 3: Comparative Full-field optical coherence tomography (FFOCT) and H&E images of neoplastic lung. (a, b) Images of adenocarcinoma of lung with lepidic-predominant pattern. Boxed areas and insets show tumor cells lining the alveolar septa. (c, d) Images of adenocarcinoma of lung with solid-predominant pattern. Boxed areas and insets shows clusters of tumor cells. (Scale bars for FFOCT: (a, c) 1 mm. Insets in (a, c) 0.1 mm. H&E total magnifications: (b, d) ×100. Insets: (b, d) ×200)

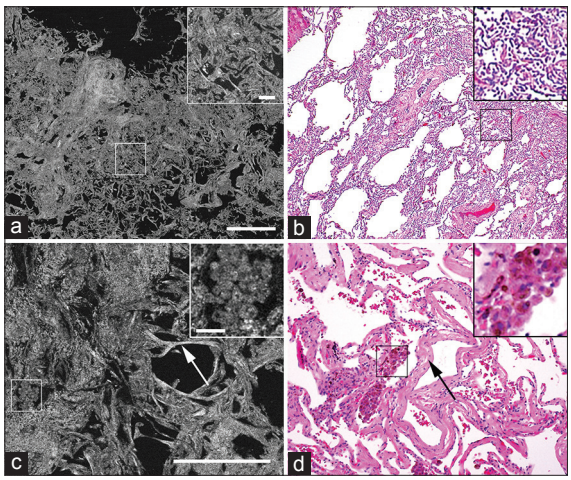

Figure 4: Comparative Full-field optical coherence tomography (FFOCT) and H&E images of non-neoplastic lung with false positive diagnosis. (a, b) Images of non-neoplastic tissue with collapse of normal lung architecture. Boxed areas and insets show dense connective tissue where it is difficult to rule out presence of tumor. (c, d) Images of non-neoplastic tissue showing clusters of smoker's macrophages (boxed areas and insets) and thickened alveolar septa (arrows). Inset shows bright spots in the cytoplasm of the macrophages, which are likely to be tar (Scale bars for FFOCT: (a) 1 mm; (c) 0.5 mm. Inset in (a) 0.1 mm; inset in C: 0.05 mm H&E total magnifications: (b) ×40 and (d) ×100. Insets: (b, d) ×200)

It is important to note that each tissue type is unique in the way it will absorb and scatter light. Thus, the depth to which a specific type of tissue can be imaged will vary depending on its constituents. We found that the most diagnostic images for human lung tissue were obtained 5-15 μm below the specimen surface. However, in certain cases (e.g., when attempting to distinguish between collapsed benign lung tissue and solid tumor), image from a single plane was found to be inadequate; and the pathologist could diagnose with greater confidence after assessing the entire image stack.

Additionally, we found that a certain amount of image post-processing significantly improved the diagnostic quality of the images. Some of the processing was routine for any microscopic image, i.e. the adjustment of brightness and contrast. This is mostly done automatically by the light-CT™ software, but manual tweaking at certain times helped highlight areas of interest (e.g., regions where there was confusion between adenocarcinoma with a lepidic pattern, vs. alveoli filled with histiocytes). Furthermore, FFOCT images are subject to speckle artifacts, similar to other imaging modalities involving interference of two images (e.g., ultrasound, OCT).[13,14] These speckles could sometimes lead to misdiagnosis, especially in situations where a pathologist is trying to distinguish between stroma and dense cellularity of solid tumor. There is an extensive literature on post-processing images to minimize speckle artifact in ultrasound, OCT and other imaging modalities.[14,15] For our images, we found that simple Gaussian filtering (also called Gaussian "blurring"; an approach that minimizes high frequency noise) was sufficient to generate images that were easier to interpret by visual inspection. However, given our high false positive

rates, further evaluation of some more sophisticated methods for speckle removal seems warranted in the future.

Based on our results and advantages offered by FFOCT, we foresee following clinical applications of this technique in the diagnosis of lung cancer:

a. FFOCT as an adjunct tool to FSA in intra-operative consultation: FFOCT can help in surgical margin assessment, especially in cases of limited lung resections, e.g. in patients with compromised lung function. The fact that FFOCT does not require any tissue processing and can generate histological quality images from fresh tissue, can help overcome the problem of freezing and sectioning artifacts observed with FSA. In addition, due to lack of sectioning, the imaged tissue can be preserved in its entirety for ancillary techniques (immunohistochemistry, genetic analysis etc.).[3] Furthermore, ability of FFOCT to generate large field images (up to 3 mm^2) at a relatively fast speed (a single plane of 2.72 mm × 2.72 mm can be acquired in ~43 s), can help speed up intra-operative decision-making[8]
b. FFOCT in obtaining diagnostically relevant tissue during biopsy procedure: By determining the adequacy of the biopsy material in freshly excised tissue before sending them to histopathology, FFOCT can reduce the number of repeat biopsies and the associated complications, such as bleeding, pneumothorax and occasional needle track seeding, as well as improve costs and time-to-decision for the patients[16]
c. FFOCT in bio-banking: FFOCT can be used for non-invasive morphological characterization of the sample and confirming that tumor is indeed present in the specimen before cryopreservation.[17]

In our study, although presence of tumor was correctly identified in all the tumor specimens, a high false positive rate was obtained for non-neoplastic lung tissue. These false positives were especially encountered in areas with extensive lung collapse or abundant smoker's macrophages, making it difficult to rule out the presence of tumor. We posit that the high false positive rates could be reduced by: (1) increased pathologist experience and sample size; (2) carrying out morphometric analysis of the images and color-coding areas of interest (e.g., cellular vs. extracellular) based on differences in texture or grayscale values in the images; (3) using fast-staining nuclear dyes (e.g. acriflavin, hematoxylin, etc.,) to distinguish tumor cells from inflammatory cells; and (4) exploring multimodal imaging approaches (e.g. combining FFOCT with fluorescence[18] etc.). In addition, imaging at higher magnification (and with a higher numerical aperture objective) might help better distinguish between adenocarcinoma cells and histiocytes based on cytologic features. This is non-trivial in an FFOCT setup, since matched objectives are used in the specimen and reference arms and thus, objectives cannot be simply switched as is possible in regular histology microscopes. Also, for any high-resolution imaging setup, there is always an effort to strike a balance between magnification and resolution on one hand and field-of-view (i.e. the size of area imaged) on the other hand (higher magnification corresponds to a more focused light beam and hence, a smaller field-of-view). This problem can be overcome, in theory, by digitally stitching (or "tiling") multiple images acquired with overlapping areas (as has been done this study); but the more the number of frames tiled, the slower the overall imaging speed would be. While the 10×/0.3 NA objective used in this study seems to be a good compromise, it may be inadequate in certain cases, where a more detailed visualization of small structures are essential for optimal diagnosis.

Although other "optical biopsy" techniques, such as OCT[11,19-23] and confocal microscopy[11,24] have been used explored in *ex vivo* and *in vivo* lung tissue imaging, each of these techniques has significant limitations at the current time. OCT provides a better depth of imaging (≥1 mm), but has a lower lateral resolution, which is insufficient to generate histology quality images. Confocal microscopy has comparable lateral resolution (≤1 μm) but somewhat worse axial resolution (~2 μm) as compared to FFOCT.[8,11] Also, confocal fluorescence microscopy typically requires exogenous contrast agents (e.g., fluorescein) and the use of relatively expensive lasers as light source. The signals are consequently limited to the structures that are labeled by the exogenous contrast agent and dissipate as the contrast agent washes out. This requirement for fluorescent contrast agent is obviated in confocal reflectance microscopy. FFOCT, on other hand, generates images from fresh (unprocessed and unstained) tissue with high lateral and axial resolution (comparable with histopathology slides).[8] A recent study compared three optical reflectance techniques, namely optical frequency domain imaging (commonly known as OCT), spectrally encoded confocal reflectance microscopy and FFOCT, to assess *ex vivo* specimens of normal rat lung. The authors found that FFOCT provided the best spatial resolution of all three techniques and suggested that it would be the best suited for assessing pathophysiological changes in the lung. The prototype system used, however, suffered from a small field of view and slow scan speed. The commercial FFOCT system used in the current study uses automated image tiling to create larger fields of view at high speed, allowing imaging of a roughly 3 mm × 3 mm tissue area in ~45 s.

CONCLUSION

The fast speed of image acquisition of a relatively large area, lack of tissue processing and associated artifacts, use of a safe light source (halogen lamp) and a user-friendly

format with small footprint, makes FFOCT an attractive potential diagnostic tool. We foresee its application as an adjunct tool to FSA during the intra-operative consultation in making binary decision (presence or absence of tumor) and for margin assessment in limited lung resection and also in tissue selection during biopsy procedure and bio-banking.

ACKNOWLEDGMENT

We acknowledge that the Light-CT™ instrument was installed as a long-term loan in the Mukherjee laboratory by LLTech, Inc. LLTech also paid part-time salary for a technician, Mr. Salamoon. None of the other authors at Weill Cornell Medical College received any compensation, monetary or otherwise; from LLTech, Inc. Claude Boccara is one of the founders of LLTech and is a part-time LLTech employee.

REFERENCES

1. Siegel R, Naishadham D, Jemal A. Cancer statistics, 2012. CA Cancer J Clin 2012;62:10-29.
2. Sienko A, Allen TC, Zander DS, Cagle PT. Frozen section of lung specimens. Arch Pathol Lab Med 2005;129:1602-9.
3. Taxy JB. Frozen section and the surgical pathologist: A point of view. Arch Pathol Lab Med 2009;133:1135-8.
4. McLaughlin SA, Ochoa-Frongia LM, Patil SM, Cody HS 3rd, Sclafani LM. Influence of frozen-section analysis of sentinel lymph node and lumpectomy margin status on reoperation rates in patients undergoing breast-conservation therapy. J Am Coll Surg 2008;206:76-82.
5. Dubois A, Boccara C. Full-field OCT. Med Sci (Paris) 2006;22:859-64.
6. Dubois A, Grieve K, Moneron G, Lecaque R, Vabre L, Boccara C. Ultrahigh-resolution full-field optical coherence tomography. Appl Opt 2004;43:2874-83.
7. Dubois A, Vabre L, Boccara AC, Beaurepaire E. High-resolution full-field optical coherence tomography with a Linnik microscope. Appl Opt 2002;41:805-12.
8. Jain M, Shukla N, Manzoor M, Nadolny S, Mukherjee S. Modified full-field optical coherence tomography: A novel tool for rapid histology of tissues. J Pathol Inform 2011;2:28.
9. Ramasamy R, Sterling J, Manzoor M, Salamoon B, Jain M, Fisher E, *et al*. Full field optical coherence tomography can identify spermatogenesis in a rodent sertoli-cell only model. J Pathol Inform 2012;3:4.
10. Wang J, Léger JF, Binding J, Boccara AC, Gigan S, Bourdieu L. Measuring aberrations in the rat brain by coherence-gated wavefront sensing using a Linnik interferometer. Biomed Opt Express 2012;3:2510-25.
11. Unglert CI, Namati E, Warger WC 2nd, Liu L, Yoo H, Kang D, *et al*. Evaluation of optical reflectance techniques for imaging of alveolar structure. J Biomed Opt 2012;17:071303.
12. Latrive A, Boccara AC. *In vivo* and *in situ* cellular imaging full-field optical coherence tomography with a rigid endoscopic probe. Biomed Opt Express 2011;2:2897-904.
13. Kremkau FW, Taylor KJ. Artifacts in ultrasound imaging. J Ultrasound Med 1986;5:227-37.
14. Ozcan A, Bilenca A, Desjardins AE, Bouma BE, Tearney GJ. Speckle reduction in optical coherence tomography images using digital filtering. J Opt Soc Am A Opt Image Sci Vis 2007;24:1901-10.
15. Mahmoud AA, El Rabaie S, Taha TE, Zahran O, Abd El-Samie FE. Comparative study of different denoising filters for speckle noise reduction in ultrasonic B mode images. Int J Image Graph Signal Proc 2013;2:1-8.
16. Smayra T, Braidy C, Menassa-Moussa L, Hlais S, Haddad-Zebouni S, Aoun N. Risk factors of pneumothorax and hemorrhage in lung biopsy: A single institution experience. J Med Liban 2012;60:4-13.
17. Dalimier E, Salomon D. Full-field optical coherence tomography: A new technology for 3D high-resolution skin imaging. Dermatology 2012;224:84-92.
18. Harms F, Dalimier E, Vermeulen P, Fragola A, Boccara AC. Multimodal full-field optical coherence tomography on biological tissue: Toward all optical digital pathology. Proc SPIE Multimodal Biomed Imaging VII 2012;8216:1-8.
19. Lam S, Standish B, Baldwin C, McWilliams A, leRiche J, Gazdar A, *et al*. *In vivo* optical coherence tomography imaging of preinvasive bronchial lesions. Clin Cancer Res 2008;14:2006-11.
20. Tsuboi M, Hayashi A, Ikeda N, Honda H, Kato Y, Ichinose S, *et al*. Optical coherence tomography in the diagnosis of bronchial lesions. Lung Cancer 2005;49:387-94.
21. Meissner S, Knels L, Schnabel C, Koch T, Koch E. Three-dimensional Fourier domain optical coherence tomography *in vivo* imaging of alveolar tissue in the intact thorax using the parietal pleura as a window. J Biomed Opt 2010;15:016030.
22. Hariri LP, Applegate MB, Mino-Kenudson M, Mark EJ, Medoff BD, Luster AD, *et al*. Volumetric optical frequency domain imaging of pulmonary pathology with precise correlation to histopathology. Chest 2013;143:64-74.
23. Liu L, Chu KK, Houser GH, Diephuis BJ, Li Y, Wilsterman EJ, *et al*. Method for quantitative study of airway functional microanatomy using micro-optical coherence tomography. PLoS One 2013;8:e54473.
24. Thiberville L, Salaün M, Lachkar S, Dominique S, Moreno-Swirc S, Vever-Bizet C, *et al*. Confocal fluorescence endomicroscopy of the human airways. Proc Am Thorac Soc 2009;6:444-9.